Clinical and pathological benefits of edaravone for Alzheimer's disease with chronic cerebral hypoperfusion in a novel mouse model

Tian Feng, Toru Yamashita, Jingwei Shang, Xiaowen Shi, Yumiko Nakano, Ryuta Morihara, Keiichiro Tsunoda, Emi Nomura, Ryo Sasaki, Koh Tadokoro, Namiko Matsumoto, Nozomi Hishikawa, Yasuyuki Ohta, and Koji Abe

Department of Neurology, Graduate School of Medicine, Dentistry and Pharmaceutical Sciences, Okayama University, 2-5-1 Shikatacho, Kitaku, Okayama 700-8558, Japan

Corresponding author: Prof. Koji Abe, Department of Neurology, Graduate School of Medicine, Dentistry and Pharmaceutical Sciences, Okayama University, 2-5-1 Shikatacho, Kitaku, Okayama 700-8558, Japan. Tel: +81-86-235-7365; Fax: +81-86-235-7368; E-mail: pgzg4jgj@s.okayama-u.ac.jp

A running headline: The treatment of edaravone to AD with CCH.

Abbreviations used: AGE, advanced glycation end products; AD, Alzheimer's disease; Aβ, amyloid-β; ALS, amyotrophic lateral sclerosis; BCCAs, bilateral common carotid arteries stenosis; CBF, cerebral blood flow; CCH, chronic cerebral hypoperfusion; CTX, cerebral cortex; DAB, diaminobenzidine; EDA, edaravone; HI, hippocampus; IL-1β, interleukin-1 beta; M, months; pTau, phosphorylated tau; PFA, paraformaldehyde; PBS, phosphate-buffered saline; NaCl, sodium chloride; NLRP3, NOD-like receptors family protein 3; ROS, reactive oxygen species; TH, thalamus; WT, wild type; 3-NT, 3-nitrotyrosine.

Abstract

Alzheimer's disease (AD) and chronic cerebral hypoperfusion (CCH) often coexist in dementia patients in aging societies. The hallmarks of AD including amyloid-β (Aβ)/phosphorylated tau (pTau) and pathology-related events such as neural oxidative stress and neuroinflammation play critical roles in pathogenesis of AD with CCH. A large number of lessons from failures of drugs targeting a single target or pathway on this so complicated disease indicate that disease-modifying therapies targeting multiple key pathways hold potent potential in therapy of the disease. In the present study, we used a novel mouse model of AD with CCH to investigate a potential therapeutic effect of a free radical scavenger, Edaravone (EDA) on AD with CCH via examining motor and cognitivie capacity, AD hallmarks, neural oxidative stress, and neuroinflammation. Compared with AD with CCH mice at 12 months of age, EDA significantly improved motor and cognitive deficits, attenuated neuronal loss, reduced Aβ/pTau accumulation, and alleviated neural oxidative stress and neuroinflammation. These findings suggest that EDA possesses clinical and pathological benefits for AD with CCH in the present mouse model and has a potential as a therapeutic agent for AD with CCH via targeting multiple key pathways of the disease pathogenesis.

Keywords: Alzheimer's disease; chronic cerebral hypoperfusion; edaravone; neuronal loss; neuroinflammation; neural oxidative stress

Introduction

Based on epidemiological analysis, Alzheimer's disease (AD) and cerebrovascular disease often coexist in dementia patients [1]. Our recent data indicated that 69% of the dementia patients who are over 75 years old suffer from AD [2], approximately 90% of whom have cerebrovascular disease [2, 3]. In cerebrovascular diseases, chronic cerebral hypoperfusion (CCH) is ubiquitous in the elderly AD patients [4-6], and could play pivotal roles in triggering and exacerbating the pathophysiological progress of AD which could be related to Aβ overproduction and accumulation [7], Aβ clearance impairment [8], Tau-hyperphosphorylation [9], neuroinflammation [10], neural oxidative stress [7], and neuronal loss [11, 12].

Despite massive progress has been made for discovering the pathogenesis of AD or AD with CCH in the recent years [13-15], No efficient disease-modifying therapeutics for AD or AD with CCH are available in clinic at present [16, 17]. According to recent lessons learnt that a therapy targeting a single protein or pathway does not have therapeutic effects on such a complex disease [17], it is necessary to discover a novel drug which can target multiple key pathways in the shared pathogenesis of AD with CCH.

Edaravone (3-methyl-1-phenyl-2pyrazoline-5-one, EDA), an oxygen radical scavenger is widely used for the treatment of acute cerebral ischemia patients [18] and amyotrophic lateral sclerosis (ALS) patients [19] owing to its anti-oxidative stress and anti-inflammation effects. Oxidative stress is a shared manifestation of AD and CCH accelerating pathogenesis including Aβ deposition, Tau-hyperphosphorylation, and inflammatory response [7, 18, 20]. Both Aβ and CCH can induce the generation of reactive oxygen species (ROS) [21, 22]. ROS is one of the crucial factors promoting the pathological progression of AD via aggregating the toxicity of Aβ

and CCH-driven vicious cycles [23, 24]. Previous studies showed that EDA not only had inhibition effects on multiple key AD pathways including Aβ, Tau-hyperphosphorylation, neuroinflammation, neural oxidative stress, and neuronal loss via scavenging both ROS and Aβ in a family AD mouse model [25] but also alleviated Aβ or streptozotocin-induced cognitive impairment via anti-oxidative stress and anti-inflammationin in rat models [26, 27] or in in-vitro models [28, 29]. Moreover, recent experimental studies also found that EDA could attenuate cognitive deficits via inhibiting oxidative stress induced by CCH in rat models [18, 30].

Therefore, in the present study, we applied a novel AD plus CCH mouse model for investigating the effects of EDA on the AD with CCH-type pathologies and behavior deficits.

Materials and Methods

Experimental model and drug treatment

All animal experiments were performed in compliance with a protocol approved by the Animal Committee of the Graduate School of Medicine and Dentistry, Okayama University (OKU#2012325). Male mice were randomly divided into 4 groups: wild type (WT) group (WT + sham surgery, n=10), APP23 group (APP23 + sham surgery, n=12), chronic cerebral hypoperfusion (CCH) group (APP23 + CCH, n=8), and edaravone (EDA)-treated group (APP23 + CCH + EDA, n=10). Transgenic mouse APP23 was previously described as the generation of the B6, D2-TgN (Thy1-APPSwe). Ameroid constrictors (0.75mm internal diameter; Research Instruments NW, Lebanon, OR, USA) was applied to induce CCH. In order to conduct a surgery of CCH, experimental mice were subjected to cervical incision, and

ameroid constrictors were applied to bilateral common carotid arteries (BCCAs) at 4 months (M) of age in the APP23 + CCH and APP23 + CCH + EDA groups. After the surgery, a single intraperitoneal injection of edaravone (50mg/kg; 3mg/ml; Mitsubishi Tanabe Pharmaceutical Co. Ltd.,) began to be administrated into mice in the APP23 + CCH + EDA group every other day till sacrifice at 12 M.

Cerebral blood flow (CBF) was measured with a laser-Doppler flowmeter (FLO-C1, Omegawave, Tokyo, Japan) before and 1, 3, 7, 14 and 28 d after the surgery. A laser Doppler flowmetry probe was fixed perpendicular to the skull 1 mm posterior and 2.5 mm lateral to the bregma where CBF values were measured five times. The mean CBF value was recorded.

Behavioral analysis

The rotarod test was performed to evaluate motor coordination and balance at 2, 5, 7, 9, 11 M-old mice by measuring latency seconds (s), as previously described [10, 31]. Rotarod speed was accelerated from 4 to 40 rpm over a 5-minute period. The latency seconds were recorded when 5 minutes had arrived or mice had fallen from a rotating drum (MK670; Muromachi Kikai Co., Tokyo, Japan). The test was repeated 5 times with an interval of 5 minutes between each trial.

An 8-arm radial maze test was used to evaluate behavioral memory (mainly for working memory) described according to our and other's reports [32, 33, 10]. In brief, each mouse was conducted a food deprivation with a schedule designed to maintain the deficiency of body weight within 10% and free access to water during 8-arm trials. For acquisition trials, maze adaptation was performed once a day in 5 consecutive days before formal trials. Five mice were allowed to explore the 8-arm maze only once for 5 minutes. Food pellets were randomly

scattered over the entire maze surface. For each formal trial, a mouse was allowed to freely make arm choices. When all four pellets had been eaten or 5 min had elapsed, the number of re-entries into the baited arms previously visited was recorded as a working memory error index. The radial maze task was performed separately when mice were 3, 6, 8, 10, and 12 M old.

Tissue preparation and immunohistochemistry

At 12 M of age, 4 mice groups were deeply anesthetized by intraperitoneal injection of pentobarbital (40mg/kg), and transcardially perfused with 20 ml of ice-cold phosphate-buffered saline (PBS) and then 20 ml of ice-cold 4% paraformaldehyde (PFA) in 0.1 mol/L phosphate buffer. The brains were removed and post-fixed in 4% PFA overnight. 50-μm-thick floating coronal sections were sliced with a vibrating blade microtome (LEICA VT1000S; Leica, Nussloch, Germany). The morphological and pathological changes were detected in the cerebral cortex (CTX), hippocampus (HI), thalamus (TH) in this study. For Nissl staining, brain sections were immersed in 0.1% cresyl violet for 5 min at room temperature, and then were dehydrated in graded alcohol, and coverslipped with microcoverglass. For single immunohistochemistry, brain sections were immerses in 0.6% periodic acid to block intrinsic peroxidase, and were treated with 5% bovine serum in 50mM PBS, pH 7.4, containing 0.1% triton to block any non-specific antibody responses then were incubated with primary antibodies. The amino acid sites were probed with the following antibodies: Aβ oligomer (1:200, F11G3; Millipore), 6E10 (1:1000, SIG-39320; Biolegend), pTau (1:200, ab64193; Abcam), 3-NT (1:200, ab61392; Abcam), AGE (1:1000, ab23722; Abcam), Iba-1 (1:1000, NCNP24; Wako), IL-1β (1:100; R&D System; AF-401-NA), NLRP3 (1:200, ab4207; Abcam), and negative control was obtained without primary antibody. Immunoreactions were visualized

using horseradish peroxidase-conjugated antibody with the diaminobenzidine reaction.

Detection and analyses

The above mentioned immunohistochemistry sections were digitized with a digital microscope camera (Olympus BX-51; Olympus Optical Co, Japan). Three levels of sections are from the caudate putamen (1.0, 0.5, and 0 mm rostal to the bregma) per brain and 3 or 4 randomly regions were selected to take photos for analysis per section (i.e., n=9-12 measurements per mouse). For the semiquantitative evaluation of Nissl, Aβ oligomer, pTau, 3-NT, AGE, Iba-1, IL-1β, and NLRP3 staining, the average pixel intensity of signal in the CTX, HI, and TH were measured. For 6E10-positive Aβ deposit analysis, data were reported as the percentage area occupied by the 6E10-positive signal in the CTX, HI, and TH. All immunostaining data were analyzed by image processing software (Image J; National Institutes of Health, Bethesda, USA).

Statistical analysis

All results were presented as mean ± SD. Statistical comparisons of LDF, rotarod test, and 8-arm test were performed using repeated measures analysis of variance (ANOVA) based on a Bonferroni's post hoc comparison. Other comparisons between two groups were tested using Mann-Whitney *u* test and among three or over three groups were tested using one way ANOVA based on a Tukey-Kramer post comparison. $p < 0.05$ was considered statistically significant.

Results

Edaravone partially recovers cortical surface CBF in AD mice with CCH

The level of CBF in APP23 group did not significantly dropped at 1 d, 3 d, 7 d, 14 d and

28 d after sham surgery (Fig. 1A, triangles). However, CBF gradually and progressively decreased in both APP23 + CCH and APP23 + CCH +EDA groups from 1 d after surgery (Fig. 1A, dotted squares and filled squares). More importantly, compared with APP23 group, the level of CBF in APP23 + CCH and APP23 + CCH +EDA groups significantly reduced at 1 d, 3 d, 7 d, 14 d and 28 d after sham surgery (Fig. 1A, #p<0.05 VS APP23, ##p<0.01 VS APP23). On the other hand, CBF in APP23 + CCH + EDA group significantly recovered at 7 d in relative to that in APP23 + CCH group, however, the value of CBF did not significantly increase at other time points but had a trend of recovery in APP23 + CCH + EDA group (Fig. 1A, &p<0.05 VS APP23 + CCH, &&p<0.01 VS APP23 + CCH).

Edaravone improves motor and cognitive deficits in AD mice with CCH

Rotarod and 8-arm radial maze tests showed no significant difference between wild type and APP23 groups at 2 M and 3 M before CCH surgery (Fig. 1B). The rotarod test demonstrated that latency was significantly shorter in APP23 + CCH group compared to WT group at 5, 7, 9 and 11 M (Fig. 1B, *p<0.05 vs WT, **p<0.01 vs WT), and in relative to APP23 group, APP23 + CCH group also showed a significantly inferior performance at a few blocks at 5, 7, 9 and 11 M (Fig. 1B, #p<0.05 vs APP23, ##p<0.01 vs APP23), indicating that motor deficits significantly existed in APP23 + CCH group at 5, 7, 9 and 11 M in our experiment. Moreover, motor performance was significantly recovered after EDA administration compared with APP23 + CCH group at a few blocks at 5, 7, 9 and 11 M (Fig. 1B, &p<0.05 VS APP23 + CCH), indicating that EDA could have an effect on the recovery of motor deficits in APP23 mice after CCH.

The 8-arm radial maze was used to examine working memory impairment. In APP23 +

CCH group, the revisiting error (used as an indicator of spatial working memory) was not significantly different among the four mice groups at 6 M (Fig. 1C). But, APP23 + CCH group showed marked difference in the number of revisiting errors in relative to WT and APP23 group at some blocks at 8, 10 and 12 M (Fig. 1C, $**p<0.01$ vs WT; $\#p<0.05$ vs APP23, $\#\#p<0.01$ vs APP23). Moreover, the number of revisiting errors is dramatically decreased at some blocks at 8, 10 and 12 M in APP23 + CCH + EDA group in comparison with APP23 + CCH group (Fig. 1C, $\&p<0.05$ VS APP23 + CCH, $\&\&p<0.01$ VS APP23 + CCH). These results indicated that spatial working memory was impaired in APP23 + CCH mice at 8, 10 and 12 M. However, EDA administration could rescue such impairment in spatial working memory.

Edaravone inhibits neuropathologic changes in AD mice with CCH

Nissl staining was used to examine neuropathologic changes in the cortex (CTX), cornu ammonis 1 (CA1), cornu ammonis 3 (CA3), dentate gyrus (DG), and thalamus (TH) of four group mice (Fig. 2A). Analysis of pixel intensity demonstrated a significant difference exist in the CA1, CA3, and DG of APP23 mice in relative to WT mice (Fig. 2B, $*p<0.05$ vs WT), moreover, compared to APP23 group at 12 M, Nissl staining intensity in APP23 + CCH group significantly decreased in the above 5 regions at 12 M (Fig. 2B, $\#p<0.05$ vs APP23, $\#\#p<0.01$ vs APP23). The dramatic decrease of Nissl staining intensity was significantly recovered in the CTX, CA1, CA3 and TH regions at 12 M by EDA treatment (Fig. 2B, $\&p<0.05$ VS APP23 + CCH, $\&\&p<0.01$ VS APP23 + CCH).

Edaravone reduces the expression of Aβ oligomer in AD mice with CCH

Aβ oligomer was labeled in the membrane and cytoplasm of cells in various brain regions, including the CTX, CA1, CA3, DG, and TH (Fig. 3A). Quantitative analysis of the pixel

intensity of Aβ oligomer-positive cells showed that the ratio of pixel intensity relative to WT group was significantly increased in the CTX, CA1, CA3, DG, TH of APP23 mice at 12 M (Fig. 3B, $^{**}p<0.01$ vs WT). Moreover, APP23 + CCH group showed a great increase of the ratio of pixel intensity of Aβ oligomer-positive cells in the above 5 regions compared to APP23 group (Fig. 3B, $^{\#\#}p<0.01$ vs APP23). These increases were significantly reduced by EDA administration (Fig. 3B, $\&\&p<0.01$ VS APP23 + CCH).

Edaravone reduces Aβ burden in AD mice with CCH

To determine the temporal expression of all forms of Aβ, we examined Aβ accumulation in the CTX, HI, and TH regions using antibody 6E10 which detects all forms of Aβ. Few 6E10-positive Aβ accumulation were observed in the CTX, HI, and TH of APP23 mice at 12 M (Fig. 3C). However, the regions of these Aβ accumulations considerably increased in APP23 + CCH group (Fig. 3D, $^{\#\#}p<0.01$ vs APP23), and EDA administration significantly reduced 6E10-positive Aβ accumulations in the CTX, HI, and TH regions at 12 M (Fig. 3D, $\&\&p<0.01$ VS APP23 + CCH).

Edaravone attenuates Tau-phosphorylation in AD mice with CCH

pTau was labeled in the cytoplasm of neural cells in the CTX, CA1, CA3, DG, and TH (Fig. 4A). Quantitative analysis of the pixel intensity of pTau-positive cells indicated that the ratio of pixel intensity relative to WT group was significantly increased in the CTX, CA3, DG, TH of APP23 mice at 12 M (Fig. 4B, $^{**}p<0.01$ vs WT). Furthermore, the ratio of pixel intensity of pTau-positive cells significantly increased in the above 5 regions of APP23 + CCH mice compared to APP23 group (Fig. 4B, $^{\#\#}p<0.01$ vs APP23). Such increases were significantly attenuated by EDA administration (Fig. 4B, $\&p<0.05$ VS APP23 + CCH, $\&\&p<0.01$ VS APP23

223 + CCH).

224 *Edaravone ameliorates neural oxidative stress in AD mice with CCH*

225 We performed studies on oxidative stress markers in the CTX, CA1, CA3, DG, and TH
226 regions among 4 group mice. 3-NT as a protein peroxidation production was clearly and mainly
227 labeled in the cytoplasm of cells in above regions at 12 M (Fig. 5A). Quantitative analysis
228 showed the level of 3-NE significantly increased in the CTX, CA1, CA3 and TH regions of
229 APP23 mice at 12 M in relative to WT mice, and the level of 3-NT was significantly reduced
230 in the above 5 regions of EDA-administrated mice compared with APP23 + CCH mice which
231 showed a significantly higher level of 3-NT intensity in the above 5 regions in comparison with
232 APP23 mice at 12 M (Fig. 5B, $^{**}p<0.01$ VS WT; $^{\#}p<0.05$ VS APP23, $^{\#\#}p<0.01$ VS APP23;
233 $\&p<0.05$ VS APP23 + CCH, $\&\&p<0.01$ VS APP23 + CCH). Furthermore, AGE as a major
234 product of oxidative degradation of glycated proteins and unsaturated fatty acids was clearly
235 and mainly labeled in the cytoplasm of cells at 12 M (Fig. 5C). We found that the pixel intensity
236 of AGE-positive signals significantly increased in the CTX, CA1, CA3, DG, and TH regions at
237 12 M comparing WT group with APP23 group, and comparing APP23 group and APP23 +
238 CCH group (Fig. 5D, $^{**}p<0.01$ VS WT; $^{\#\#}p<0.01$ VS APP23). More importantly, EDA
239 administration could significantly ameliorate such increased level of AGE expression in the
240 above 5 regions of APP23 + CCH at 12 M (Fig. 5D, $\&p<0.05$ VS APP23 + CCH, $\&\&p<0.01$
241 VS APP23 + CCH).

242 *Edaravone ameliorates neuroinflammation in AD mice with CCH*

243 The expression of Iba-1-positive microglial cells was clearly observed in the CTX, CA1,
244 CA3, DG, and TH regions at 12 M (Fig. 6A). Quantitative analysis indicated the ratio of pixel

intensity in comparison with WT group was significantly increased in the above 5 regions of APP23 mice at 12 M, and APP23 + CCH group showed a remarkable increase of Iba-1-positive microglia intensity in the above 5 regions at 12 M in relative to APP23 mice (Fig. 6B, #p<0.05 VS APP23, ##p<0.01 VS APP23; #p<0.05 VS APP23, ##p<0.01 VS APP2). EDA administration strongly ameliorate such activation of microglia in above regions at 12 M (Fig. 6B, &p<0.05 VS APP23 + CCH, &&p<0.01 VS APP23 + CCH).

IL-1β showed a strongly increased expression in the neural cytoplasm of three APP23 groups, especially in APP23 + CCH group in the CTX, CA1, CA3, DG, and TH regions at 12 M (Fig. 6C). Quantitative analysis demonstrated that the ratio of pixel intensity in APP23 group is significantly higher than that in WT group in the above 5 regions at 12 M, and APP23 mice with CCH presented the strongest expression of IL-1β-positive signals among three APP23 groups in the above 5 regions at 12 M, which was greatly attenuated by EDA administration (Fig. 6D, *p<0.05 VS WT, **p<0.01 VS WT; #p<0.05 VS APP23, ##p<0.01 VS APP23; &p<0.05 VS APP23 + CCH, &&p<0.01 VS APP23 + CCH).

The NLRP3 as an intracellular protein is an important part of inflammasome complexes, involving many chronic neurological diseases such as AD and CCH. In our present study, compared with WT group, the expression of NLRP3 displayed stronger positive signals in cellular cytoplasm of the CTX, CA1, CA3, DG, and TH regions in three APP23 groups at 12 M (Fig. 6E). Analysis of pixel intensity showed a significantly increased expression of NLRP3 in APP23 group compared to WT group in the above 5 regions at 12 M compared with WT group (Fig. 6F, *p<0.05 VS WT, **p<0.01 VS WT). Additionally, CCH dramatically accelerated the expression of NLRP3 in the above 5 regions of APP23 mice (Fig. 6F, #p<0.05

VS APP23, ##p<0.01 VS APP23). More importantly, our result showed that EDA administration could have an effect on ameliorating such increased expression in above regions at 12 M (Fig. 6F, &p<0.05 VS APP23 + CCH, &&p<0.01 VS APP23 + CCH).

Discussion

In the present study, we found that EDA can partly improved CBF, ameliorated neuropathologic damage, reduced Aβ/Tau-phosphorylation (pTau) aggregation, ameliorated neural oxidative stress and neuroinflammation, and, more importantly, improved motor and cognitive deficits in AD with CCH mice at 12 M, indicating that EDA as a free radical scavenger could be a potential drug for the treatment of AD with CCH commonly observed in the elder society worldwide.

A free radical scavenger, EDA has been shown not only to improve the decrease of CBF and motor and cognitive deficits in rats with CCH [18] but also to ameliorate cognitive impairment in a familial AD mouse model [25]. In the present study, we first examined the effect of EDA on oligemia and behavioral deficits in an AD plus CCH mouse model that is first reported in our previous study [10]. The present AD plus CCH mouse model showed a slowly progressive decrease of CBF, which was partly recovered by EDA administration (Fig. 1), and analyses of behavior tests showed better both motor performance and cognitive performance in APP23 + AD + EDA group at 5, 7, 9, 11 M and 8, 10, 12 M, respectively (Fig. 1), indicating that EDA could have a potent effect on improving motor and cognitive deficits in AD with CCH mice. Next, we were determined to detect the effect of EDA administration on celluar and molecular changes which is involved in AD with CCH. In our previous study, CCH accelerated

motor and cognitive deficits with strong neuronal loss in APP23 mice at 12 M, which could be due to massive reactive oxygen species and inflammatory responses induced by Aβ/pTau toxiety and neuronal energy failure [34]. The present study showed that EDA had a strong neuroprotection on ameliorating neuronal loss in CTX, CA1, CA3, and TH regions of APP23 + CCH mice at 12 M (Fig. 2). According to previous papers, EDA could exert a neuroprotection via scavenging Aβ/pTau in AD animal models [25]. Moreover, massive Aβ/pTau accumulation is also a key manifestations of CCH disease [35]. Therefore, we suppose that EDA could alleviate neuronal loss and neurodegeration in AD with CCH mice through reducing Aβ/pTau expression. For verifying our hypothesis, we examined the effect of EDA on alterations of Aβ oligomer, total Aβ, and pTau expressions in APP23 + CCH mice at 12 M. The results show that EDA strongly ameliorated Aβ/pTau aggregation exacerbated by CCH in APP23 mice at 12 M (Figs. 3, 4). Furthermore, some previous studies showed that before or after the onset of Aβ/pTau deposition in the condition of CCH, neural oxidative stress and neuroinflammation progressively occur and dramatically accelerate the pathological progression of AD by inducing an abnormally multiple of Aβ/pTau expression [36-40]. Therefore, we examined the effect of EDA on neural oxidative stress and neuroinflammation in AD with CCH mice at 12 M by analysing changes of neural oxidative stress markers 3-NT (a protein peroxidation product) and AGE (an oxidative glycated product), and neuroinflammation markers Iba-1 (microglia), Il-1β (proinflammatory cytokines), and NLRP3 (inflammasome), respectively. The results (Figs. 5,6) indicated that EDA could dramatically suppress neural oxidative stress and neuroinflammation enhanced by CCH in APP23 mice at 12 M. Overall, EDA could improve motor and cognitive impairments by alleviating neuronal loss perhaps owing to its effect of decreasing Aβ/pTau

accumulations, neural oxidative stress, and neuroinflammation in APP23 + CCH mice model at 12 M.

In summary, the present study demonstrated a strong potential of ischemic stroke drug EDA in the therapy for AD with CCH which is commonly observed in current elder societies woeldwide [41] by targeting multiple key pathways, including neuropathologic damage, Aβ/pTau aggregation, neuronal oxidative stress, and neuroinflammation, which presents a future research direction of disease-modifying therapy applied in AD with CCH by simultaneously inhibiting multiple cascades involving in disease pathogenesis.

Acknowledgements

This work was partly supported by Grant-in-Aid for Scientific Research (B) 25293202, (C) 15K09316 and Challenging Research 15K15527 and Young Research 15K21181, and by Grants-in-Aid from the Research Committees (Mizusawa H, Nakashima K, Nishizawa M, Sasaki H, and Aoki M) from the Ministry of Health, Labour and Welfare of Japan. We are grateful to Mitsubishi Tanabe Pharma (Osaka, Japan) for the gift of the edaravone.

Conflict of Interest

The authors declare no potential conflicts of interest.

References

[1] Yang H, Hou T, Wang W, Luo Y, Yan F, Jia J (2018) The Effect of Chronic Cerebral Hypoperfusion on Amyloid-β Metabolism in a Transgenic Mouse Model of Alzheimer's

Disease (PS1V97L). *Journal of Alzheimer's Disease* **62**, 1609-1621.

[2] Hishikawa N, Fukui Y, Sato K, Kono S, Yamashita T, Ohta Y, Deguchi K, Abe K (2015) Characteristic features of cognitive, affective and daily living functions of late-elderly dementia. *Geriatrics & Gerontology International* **16**, 458-465.

[3] Kisler K, Nelson AR, Montagne A, Zlokovic BV (2017) Cerebral blood flow regulation and neurovascular dysfunction in Alzheimer disease. *Nature reviews. Neuroscience* **18**, 419-434.

[4] Bertsch K, Hagemann D, Hermes M, Walter C, Khan R, Naumann E (2009) Resting cerebral blood flow, attention, and aging. *Brain Research* **1267**, 77-88.

[5] Chen W, Song X, Beyea S, D'Arcy R, Zhang Y, Rockwood K (2011) Advances in perfusion magnetic resonance imaging in Alzheimer's disease. *Alzheimer's & Dementia* **7**, 185-196.

[6] Mazza M, Marano G, Traversi G, Bria P, Mazza S (2011) Primary Cerebral Blood Flow Deficiency and Alzheimer's Disease: Shadows and Lights. *Journal of Alzheimer's Disease* **23**, 375-389.

[7] Feng T, Yamashita T, Zhai Y, Shang J, Nakano Y, Morihara R, Fukui Y, Hishikawa N, Ohta Y, Abe K (2018) Chronic cerebral hypoperfusion accelerates Alzheimer's disease pathology with the change of mitochondrial fission and fusion proteins expression in a novel mouse model. *Brain Research* **1696**, 63-70.

[8] Ashok A, Rai NK, Raza W, Pandey R, Bandyopadhyay S (2016) Chronic cerebral hypoperfusion-induced impairment of Aβ clearance requires HB-EGF-dependent sequential activation of HIF1α and MMP9. *Neurobiology of Disease* **95**, 179-193.

[9] Bloom GS (2014) Amyloid-β and tau: The trigger and bullet in alzheimer disease pathogenesis. *JAMA Neurology* **71**, 505-508.

[10] Zhai Y, Yamashita T, Nakano Y, Sun Z, Shang J, Feng T, Morihara R, Fukui Y, Ohta Y, Hishikawa N, Abe K (2016) Chronic Cerebral Hypoperfusion Accelerates Alzheimer's Disease Pathology with Cerebrovascular Remodeling in a Novel Mouse Model. *Journal of Alzheimer's Disease* **53**, 893-905.

[11] Kwon KJ, Lee EJ, Kim MK, Kim SY, Kim JN, Kim JO, Kim H-J, Kim HY, Han J-S, Shin CY, Han S-H (2015) Diabetes augments cognitive dysfunction in chronic cerebral hypoperfusion by increasing neuronal cell death: Implication of cilostazol for diabetes mellitus-induced dementia. *Neurobiology of Disease* **73**, 12-23.

[12] Shang J, Yamashita T, Zhai Y, Nakano Y, Morihara R, Fukui Y, Hishikawa N, Ohta Y, Abe K (2016) Strong Impact of Chronic Cerebral Hypoperfusion on Neurovascular Unit, Cerebrovascular Remodeling, and Neurovascular Trophic Coupling in Alzheimer's Disease Model Mouse. *Journal of Alzheimer's Disease* **52**, 113-126.

[13] Golde TE, Koo EH, Felsenstein KM, Osborne BA, Miele L (2013) γ-Secretase inhibitors and modulators. *Biochimica et biophysica acta* **1828**, 2898-2907.

[14] Liu Y-H, Giunta B, Zhou H-D, Tan J, Wang Y-J (2012) Immunotherapy for Alzheimer disease—the challenge of adverse effects. *Nature Reviews Neurology* **8**, 465.

[15] Yan R, Vassar R (2014) Targeting the β secretase BACE1 for Alzheimer's disease therapy. *The Lancet. Neurology* **13**, 319-329.

[16] Matsuzono K, Hishikawa N, Takao Y, Wakutani Y, Yamashita T, Deguchi K, Abe K (2015) Combination benefit of cognitive rehabilitation plus donepezil for Alzheimer's

disease patients. *Geriatrics & Gerontology International* **16**, 200-204.

[17] Wang Y-J (2014) Lessons from immunotherapy for Alzheimer disease. *Nature Reviews Neurology* **10**, 188.

[18] Ueno Y, Zhang N, Miyamoto N, Tanaka R, Hattori N, Urabe T (2009) Edaravone attenuates white matter lesions through endothelial protection in a rat chronic hypoperfusion model. *Neuroscience* **162**, 317-327.

[19] Abe K, Aoki M, Tsuji S, Itoyama Y, Sobue G, Togo M, Hamada C, Tanaka M, Akimoto M, Nakamura K, Takahashi F, Kondo K, Yoshino H, Abe K, Aoki M, Tsuji S, Itoyama Y, Sobue G, Togo M, Hamada C, Sasaki H, Yabe I, Doi S, Warita H, Imai T, Ito H, Fukuchi M, Osumi E, Wada M, Nakano I, Morita M, Ogata K, Maruki Y, Ito K, Kano O, Yamazaki M, Takahashi Y, Ishiura H, Ogino M, Koike R, Ishida C, Uchiyama T, Mizoguchi K, Obi T, Watanabe H, Atsuta N, Aiba I, Taniguchi A, Sawada H, Hazama T, Fujimura H, Kusaka H, Kunieda T, Kikuchi H, Matsuo H, Ueyama H, Uekawa K, Tanaka M, Akimoto M, Ueda M, Murakami A, Sumii R, Kudou T, Nakamura K, Morimoto K, Yoneoka T, Hirai M, Sasaki K, Terai H, Natori T, Matsui H, Kotani K, Yoshida K, Iwasaki T, Takahashi F, Kondo K, Yoshino H (2017) Safety and efficacy of edaravone in well defined patients with amyotrophic lateral sclerosis: a randomised, double-blind, placebo-controlled trial. *The Lancet Neurology* **16**, 505-512.

[20] Washida K, Ihara M, Nishio K, Fujita Y, Maki T, Yamada M, Takahashi J, Wu X, Kihara T, Ito H, Tomimoto H, Takahashi R (2010) Nonhypotensive Dose of Telmisartan Attenuates Cognitive Impairment Partially Due to Peroxisome Proliferator-Activated Receptor-γ Activation in Mice With Chronic Cerebral Hypoperfusion. *Stroke* **41**, 1798-

1806.

[21] Cheignon C, Tomas M, Bonnefont-Rousselot D, Faller P, Hureau C, Collin F (2017) Oxidative stress and the amyloid beta peptide in Alzheimer's disease. *Redox biology* **14**, 450-464.

[22] Du J, Ma M, Zhao Q, Fang L, Chang J, Wang Y, Fei R, Song X (2013) Mitochondrial bioenergetic deficits in the hippocampi of rats with chronic ischemia-induced vascular dementia. *Neuroscience* **231**, 345-352.

[23] Choi D-H, Lee K-H, Kim J-H, Seo J-H, Kim HY, Shin CY, Han J-S, Han S-H, Kim Y-S, Lee J (2014) NADPH oxidase 1, a novel molecular source of ROS in hippocampal neuronal death in vascular dementia. *Antioxidants & redox signaling* **21**, 533-550.

[24] Zawia NH, Lahiri DK, Cardozo-Pelaez F (2009) Epigenetics, oxidative stress, and Alzheimer disease. *Free radical biology & medicine* **46**, 1241-1249.

[25] Jiao S-S, Yao X-Q, Liu Y-H, Wang Q-H, Zeng F, Lu J-J, Liu J, Zhu C, Shen L-L, Liu C-H, Wang Y-R, Zeng G-H, Parikh A, Chen J, Liang C-R, Xiang Y, Bu X-L, Deng J, Li J, Xu J, Zeng Y-Q, Xu X, Xu H-W, Zhong J-H, Zhou H-D, Zhou X-F, Wang Y-J (2015) Edaravone alleviates Alzheimer's disease-type pathologies and cognitive deficits. *Proceedings of the National Academy of Sciences* **112**, 5225.

[26] Yang R, Wang Q, Li F, Li J, Liu X (2015) Edaravone injection ameliorates cognitive deficits in rat model of Alzheimer's disease. *Neurological Sciences* **36**, 2067-2072.

[27] Zhou S, Yu G, Chi L, Zhu J, Zhang W, Zhang Y, Zhang L (2013) Neuroprotective effects of edaravone on cognitive deficit, oxidative stress and tau hyperphosphorylation induced by intracerebroventricular streptozotocin in rats. *NeuroToxicology* **38**, 136-145.

[28] Liu J-f, Yan X-d, Qi L-s, Li L, Hu G-y, Li P, Zhao G (2015) Ginsenoside Rd attenuates Aβ25–35-induced oxidative stress and apoptosis in primary cultured hippocampal neurons. *Chemico-Biological Interactions* **239**, 12-18.

[29] Zhang G-l, Zhang W-g, Du Y, Yao L, Sun H, Zhang R, Liu E, Bu N, Wu H-q, Zhang L, Li T-t, Guo Y-y (2013) Edaravone Ameliorates Oxidative Damage Associated with Aβ25-35 Treatment in PC12 Cells. *Journal of Molecular Neuroscience* **50**, 494-503.

[30] Miyamoto N, Maki T, Pham L-DD, Hayakawa K, Seo JH, Mandeville ET, Mandeville JB, Kim K-W, Lo EH, Arai K (2013) Oxidative stress interferes with white matter renewal after prolonged cerebral hypoperfusion in mice. *Stroke* **44**, 3516-3521.

[31] Ohta Y, Nagai M, Nagata T, Murakami T, Nagano I, Narai H, Kurata T, Shiote M, Shoji M, Abe K (2006) Intrathecal injection of epidermal growth factor and fibroblast growth factor 2 promotes proliferation of neural precursor cells in the spinal cords of mice with mutant human SOD1 gene. *Journal of Neuroscience Research* **84**, 980-992.

[32] Kurata T, Miyazaki K, Kozuki M, Panin V-L, Morimoto N, Ohta Y, Nagai M, Ikeda Y, Matsuura T, Abe K (2011) Atorvastatin and pitavastatin improve cognitive function and reduce senile plaque and phosphorylated tau in aged APP mice. *Brain Research* **1371**, 161-170.

[33] Okada M, Tamura A, Urae A, Nakagomi T, Kirino T, Mine K, Fujiwara M (1995) Long-Term Spatial Cognitive Impairment following Middle Cerebral Artery Occlusion in Rats. A Behavioral Study. *Journal of Cerebral Blood Flow & Metabolism* **15**, 505-512.

[34] Di Marco LY, Venneri A, Farkas E, Evans PC, Marzo A, Frangi AF (2015) Vascular dysfunction in the pathogenesis of Alzheimer's disease — A review of endothelium-

443 mediated mechanisms and ensuing vicious circles. *Neurobiology of Disease* **82**, 593-
444 606.
445 [35] Daulatzai MA (2016) Cerebral hypoperfusion and glucose hypometabolism: Key
446 pathophysiological modulators promote neurodegeneration, cognitive impairment, and
447 Alzheimer's disease. *Journal of Neuroscience Research* **95**, 943-972.
448 [36] Bonet-Costa V, Pomatto LC-D, Davies KJA (2016) The Proteasome and Oxidative
449 Stress in Alzheimer's Disease. *Antioxidants & redox signaling* **25**, 886-901.
450 [37] Chen Z, Zhong C (2014) Oxidative stress in Alzheimer's disease. *Neuroscience bulletin*
451 **30**, 271-281.
452 [38] Fang Y, Yao L, Li C, Wang J, Wang J, Chen S, Zhou X-F, Liao H (2016) The blockage
453 of the Nogo/NgR signal pathway in microglia alleviates the formation of Aβ plaques
454 and tau phosphorylation in APP/PS1 transgenic mice. *Journal of neuroinflammation* **13**,
455 56-56.
456 [39] Grimaldi A, Brighi C, Peruzzi G, Ragozzino D, Bonanni V, Limatola C, Ruocco G, Di
457 Angelantonio S (2018) Inflammation, neurodegeneration and protein aggregation in the
458 retina as ocular biomarkers for Alzheimer's disease in the 3xTg-AD mouse model. *Cell*
459 *death & disease* **9**, 685-685.
460 [40] McGeer PL, Rogers J, McGeer EG (2016) Inflammation, Antiinflammatory Agents, and
461 Alzheimer’s Disease: The Last 22 Years. *Journal of Alzheimer's Disease* **54**, 853-857.
462 [41] Tokuchi R, Hishikawa N, Kurata T, Sato K, Kono S, Yamashita T, Deguchi K, Abe K
463 (2014) Clinical and demographic predictors of mild cognitive impairment for
464 converting to Alzheimer's disease and reverting to normal cognition. *Journal of the*

Neurological Sciences **346**, 288-292.

Figure Legends

Fig. 1. Temporal profiles of cerebral blood flow (CBF) in APP23 mice and APP23 mice after implantation of ameroid constrictors with or without edaravone (EDA) administration. The levels of CBF at indicated time points (pre-operation, and 1, 3, 7, 14, 28 days after each surgery) are shown as percentage of the baseline CBF (A). EDA administration attenuates cerebral chronic hypoperfusion (CCH)-induced motor and memory deficits (B and C). Motor (Rotarod) and memory (8-arm radial maze) functions before and after CCH. Mean time of the latency indicates motor capacity in rotarod test. Note progressively inferior motor performances in the APP23 + CCH group than in the wild type (WT) group and APP23 group (B). The mean number of re-entry choices indicates working memory capacity in 8-arm test. Note gradually increased errors in the APP23 + CCH group that in the WT group and APP23 group (C). EDA administration dramatically rescued such motor and memory deficits (B and C) (*p<0.05 vs WT, **p<0.01 vs WT; #p<0.05 vs APP23, ##p<0.01 vs APP23; &p<0.05 VS APP23 + CCH, &&p<0.01 VS APP23 + CCH).

Fig. 2. EDA inhibits neuronal loss in AD + CCH mice at 12 M. Representative photomicrographs of nissl staining in the cerebral cortex (CTX), cornu ammonis 1 (CA1), cornu ammonis 3 (CA3), dentate gyrus (DG), and thalamus (TH) at 12 M (A). Quantitative analysis of nissl staining intensity in the CTX, CA1, CA3, and TH at 12 M (B) (*p<0.05 vs WT; #p<0.05 vs APP23, ##p<0.01 vs APP23; &p<0.05 VS APP23 + CCH, &&p<0.01 VS APP23 + CCH.

Scale bar=50 μm).

Fig. 3. EDA reduces the expression of Aβ oligomer in APP23 + CCH mice at 12 M. Representative photomicrographs of Aβ oligomer (A) and quantitative analysis of Aβ oligomer-positive neural cell pixel intensity (B) in the CTX, CA1, CA3, DG, and TH at 12 M. EDA reduces Aβ burdens in APP23 + CCH mice at 12 M. Representative photomicrographs of all forms of Aβ burdens (C) and quantitative analysis of Aβ burdens areas (D) in the CTX, hippocampus (HI) and TH at 12 M (**p<0.01 vs WT; ##p<0.01 vs APP23; &&p<0.01 VS APP23 + CCH. Scale bar=50 μm).

Fig. 4. EDA attenuates the expression of phosphorylated tau (pTau) in APP23 + CCH mice at 12 M. Representative photomicrographs of pTau (A) and quantitative analysis of pTau-positive neural cell pixel intensity (B) in the CTX, CA1, CA3, DG, and TH at 12 M (**p<0.01 vs WT; ##p<0.01 vs APP23; &p<0.05 VS APP23 + CCH, &&p<0.01 VS APP23 + CCH. Scale bar=50 μm).

Fig. 5. EDA ameliorates neural oxidative stress in AD + CCH mice at 12 M. Representative photomicrographs of 3-NT (A) and AGE (C) in the CTX, CA1, CA3, DG, and TH at 12 M. Quantitative analysis of 3-NT-positive neural cell pixel intensity (B) and AGE-positive neural cell pixel intensity (D) in the CTX, CA1, CA3, DG, and TH at 12 M (**p<0.01 vs WT; #p<0.05 vs APP23, ##p<0.01 vs APP23; &p<0.05 VS APP23 + CCH, &&p<0.01 VS APP23 + CCH. Scale bar=50 μm).

Fig. 6. EDA ameliorates neuroinflammation in APP23 + CCH mice at 12 M. Representative photomicrographs of Iba-1 (A), IL-1β (C), and NLRP3 (E) in the CTX, CA1, CA3, DG, and TH at 12 M. Quantitative analysis of Iba-1-positive microglia pixel intensity (B), IL-1β-positive neural cell pixel intensity (D), and NLRP3-positive neural cell pixel intensity (F) in the CTX, CA1, CA3, DG, and TH at 12 M (*p<0.05 vs WT, **p<0.01 vs WT; #p<0.05 vs APP23, ##p<0.01 vs APP23; &p<0.05 VS APP23 + CCH, &&p<0.01 VS APP23 + CCH. Scale bar=50 μm).

Fig. 1

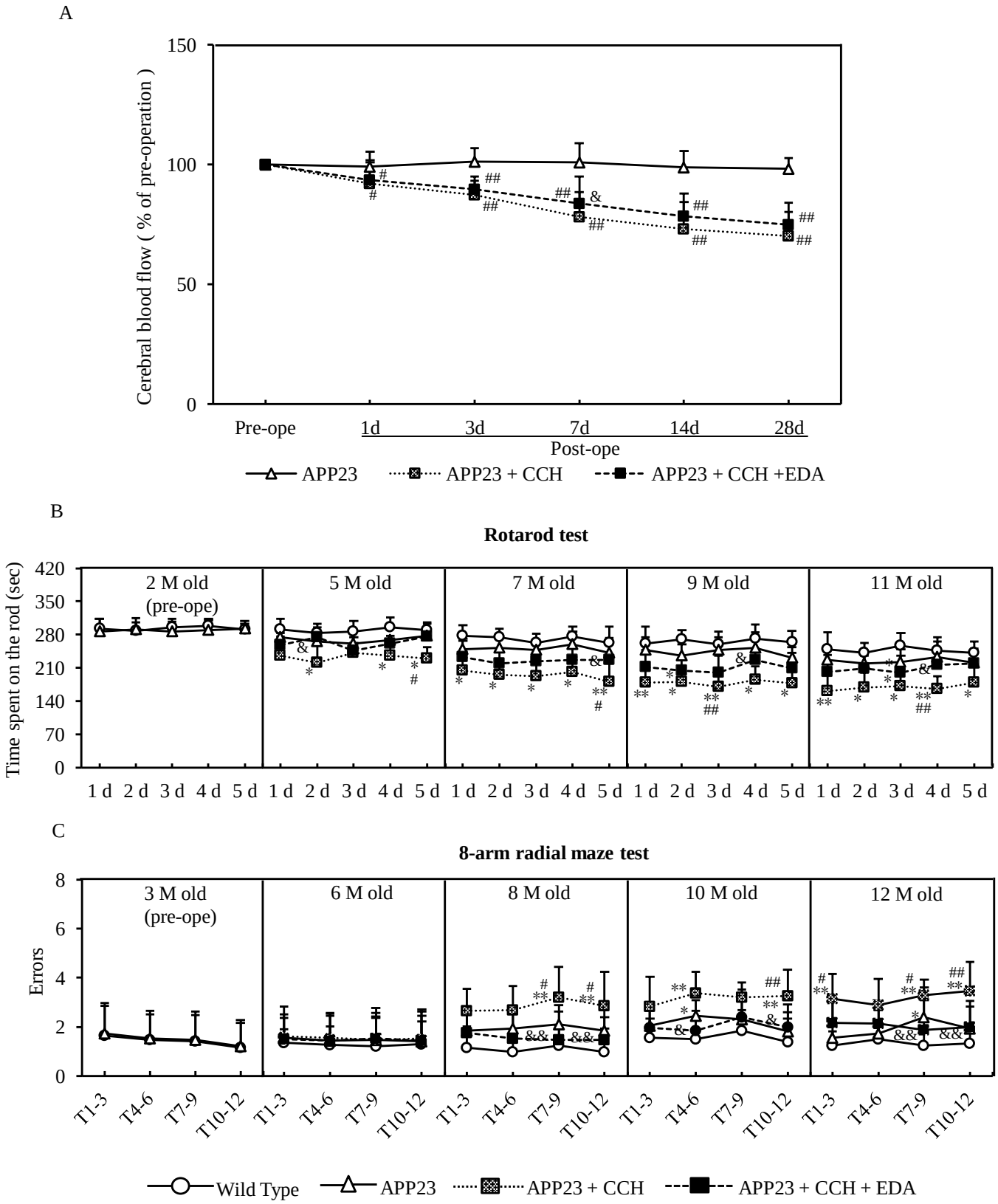
A
Cerebral blood flow (% of pre-operation)
150
100
50
0
Pre-ope
1d
3d
7d
14d
28d
Post-ope
APP23
APP23 + CCH
APP23 + CCH +EDA
B
Rotarod test
Time spent on the rod (sec)
420
350
280
210
140
70
0
2 M old
(pre-ope)
5 M old
7 M old
9 M old
11 M old
1 d 2 d 3 d 4 d 5 d
C
8-arm radial maze test
Errors
8
6
4
2
0
3 M old
(pre-ope)
6 M old
8 M old
10 M old
12 M old
T1-3
T4-6
T7-9
T10-12
Wild Type
APP23
APP23 + CCH
APP23 + CCH + EDA

Fig. 2

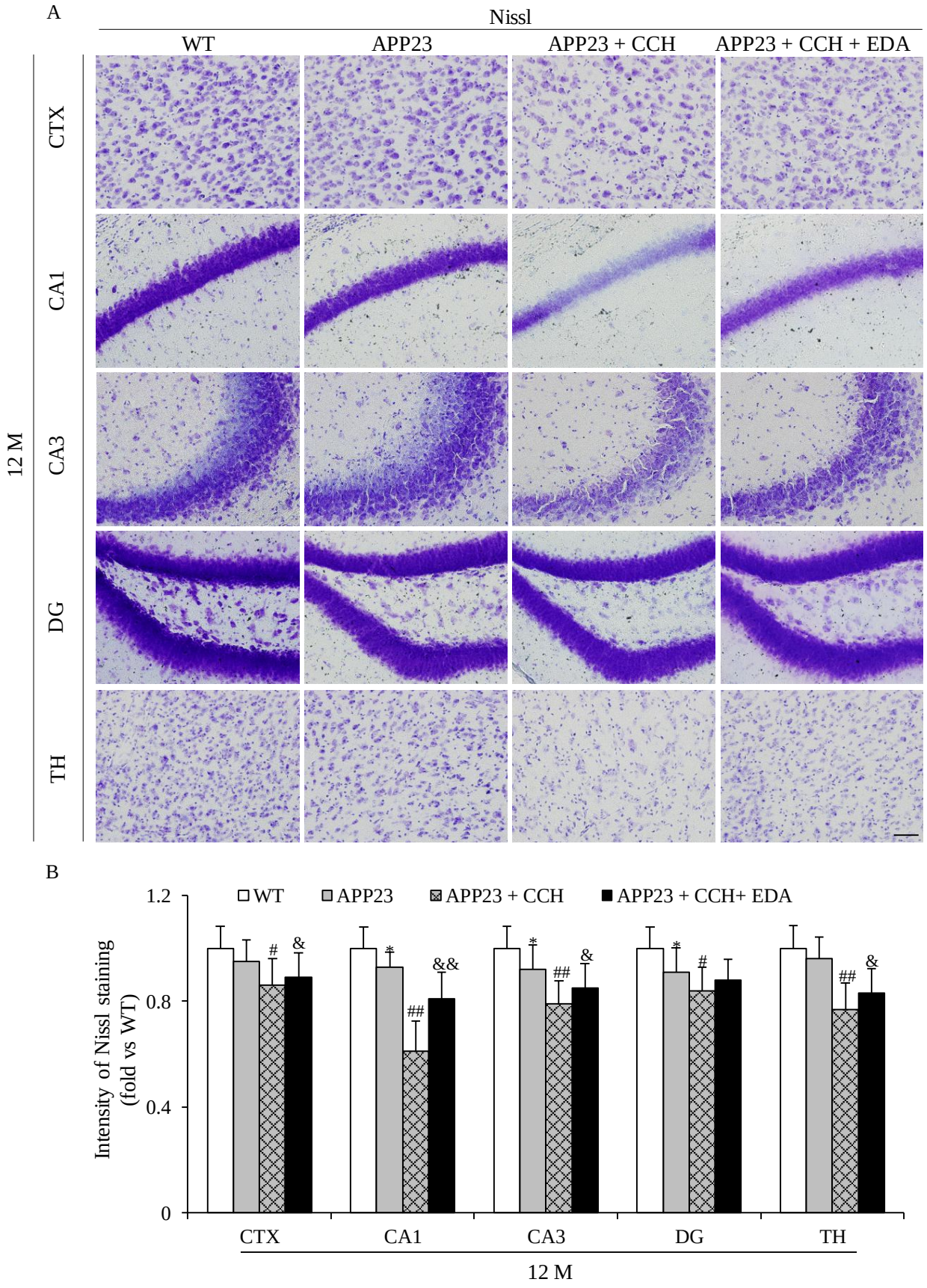
A
Nissl
WT
APP23
APP23 + CCH
APP23 + CCH + EDA
12 M
CTX
CA1
CA3
DG
TH
B
WT
APP23
APP23 + CCH
APP23 + CCH+ EDA
Intensity of Nissl staining
(fold vs WT)
1.2
0.8
0.4
0
CTX
CA1
CA3
DG
TH
12 M

Fig. 3

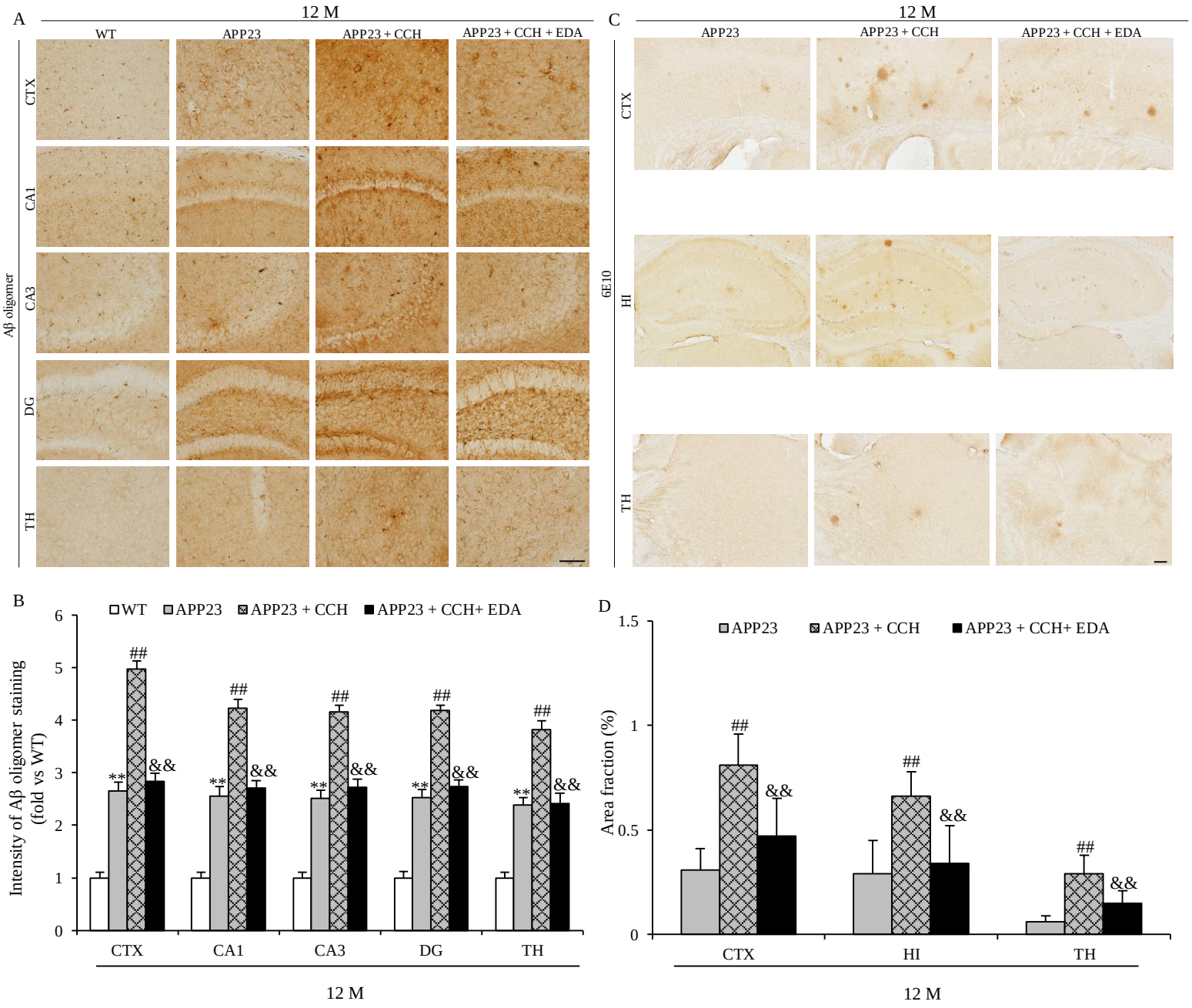
A
12 M
WT
APP23
APP23 + CCH
APP23 + CCH + EDA
CTX
CA1
CA3
DG
TH
Aβ oligomer
C
12 M
APP23
APP23 + CCH
APP23 + CCH + EDA
CTX
HI
TH
6E10
B
WT
APP23
APP23 + CCH
APP23 + CCH+ EDA
Intensity of Aβ oligomer staining (fold vs WT)
CTX
CA1
CA3
DG
TH
12 M
D
APP23
APP23 + CCH
APP23 + CCH+ EDA
Area fraction (%)
CTX
HI
TH
12 M

Fig. 4

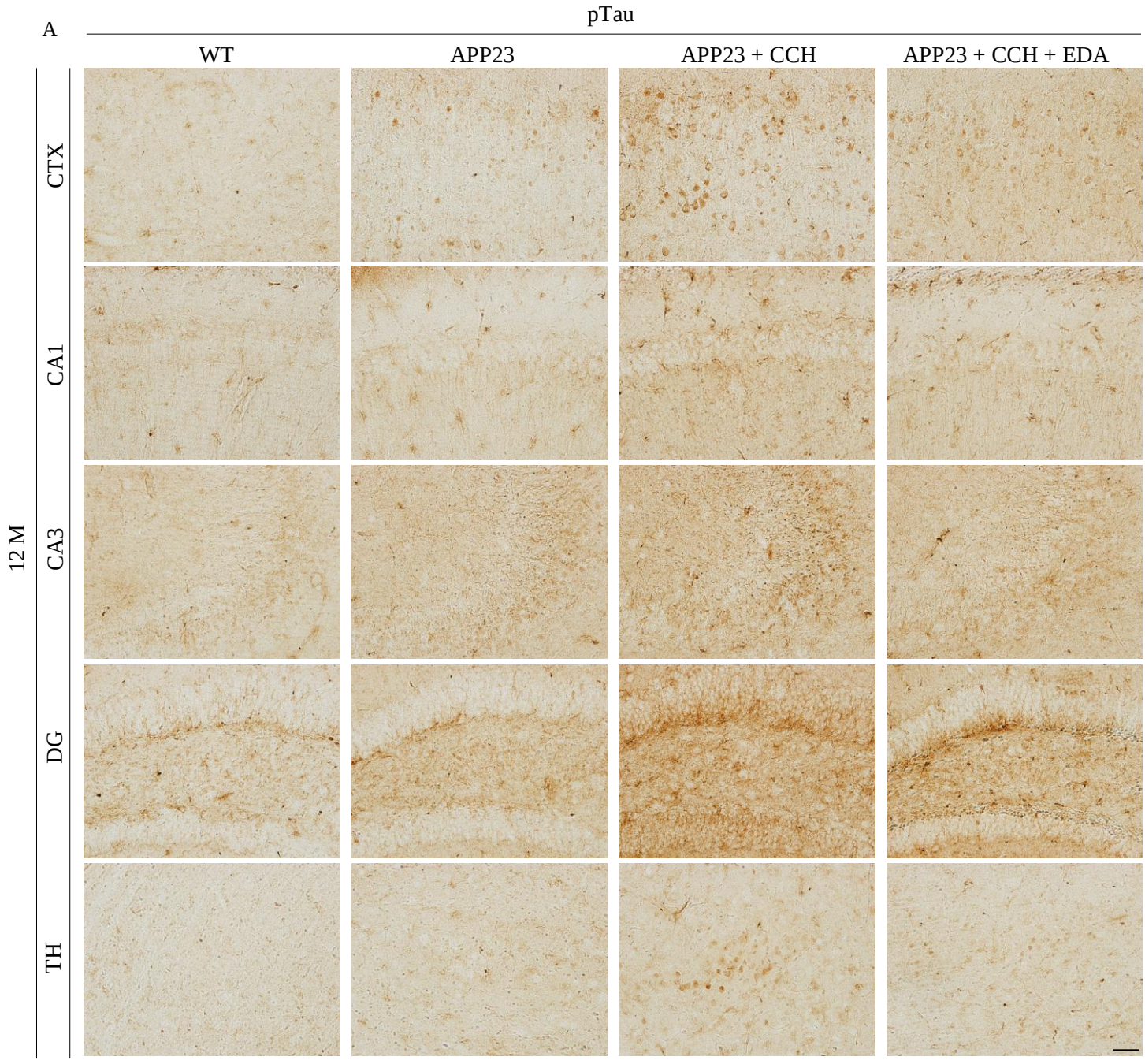
A
pTau
WT
APP23
APP23 + CCH
APP23 + CCH + EDA
12 M
CTX
CA1
CA3
DG
TH

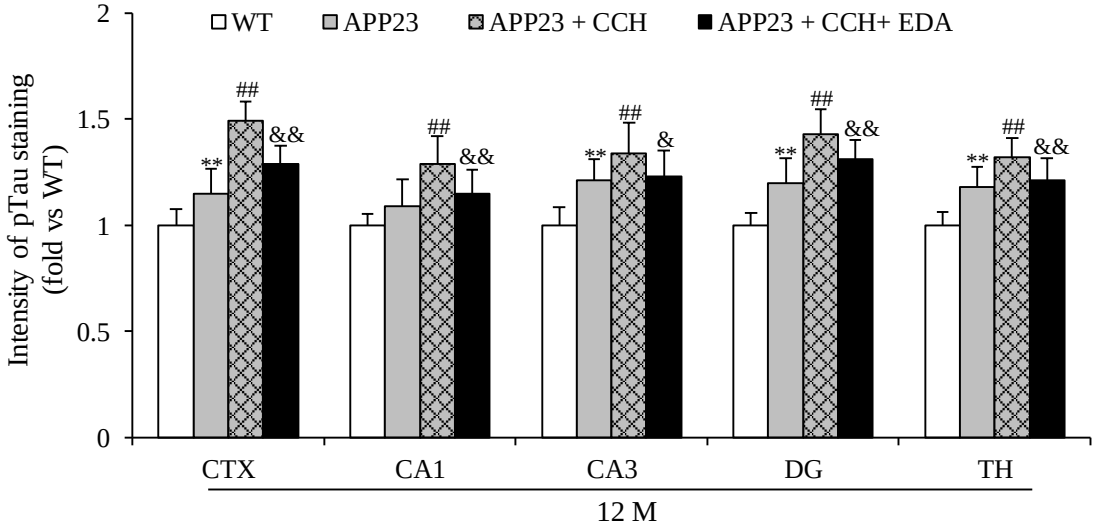
B
WT
APP23
APP23 + CCH
APP23 + CCH+ EDA
Intensity of pTau staining (fold vs WT)
2
1.5
1
0.5
0
**
##
&&
&
CTX
CA1
CA3
DG
TH
12 M

Fig. 5

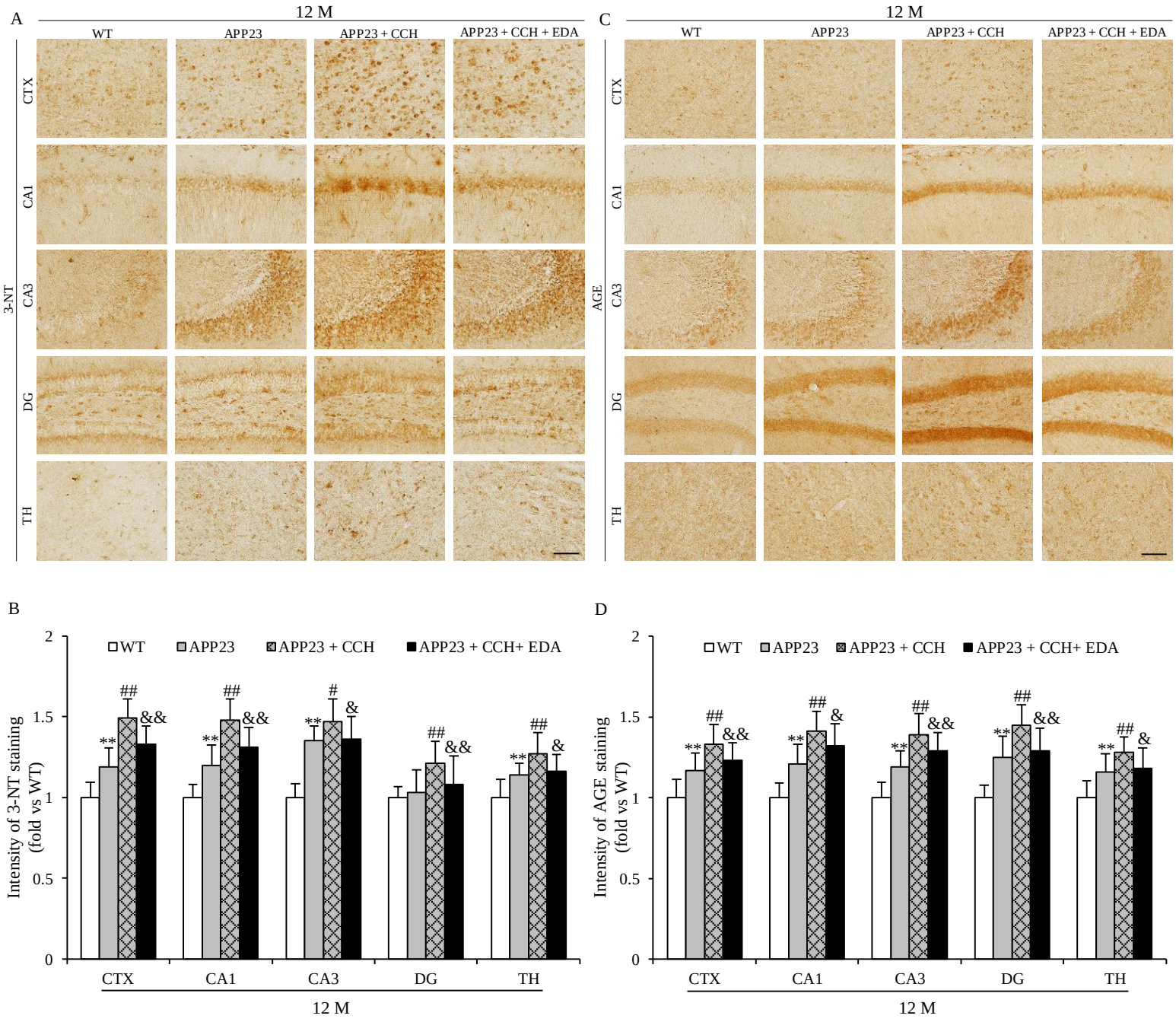
A
12 M
WT
APP23
APP23 + CCH
APP23 + CCH + EDA
CTX
CA1
CA3
DG
TH
3-NT
C
AGE
B
Intensity of 3-NT staining (fold vs WT)
D
Intensity of AGE staining (fold vs WT)
WT
APP23
APP23 + CCH
APP23 + CCH+ EDA
12 M

Fig. 6

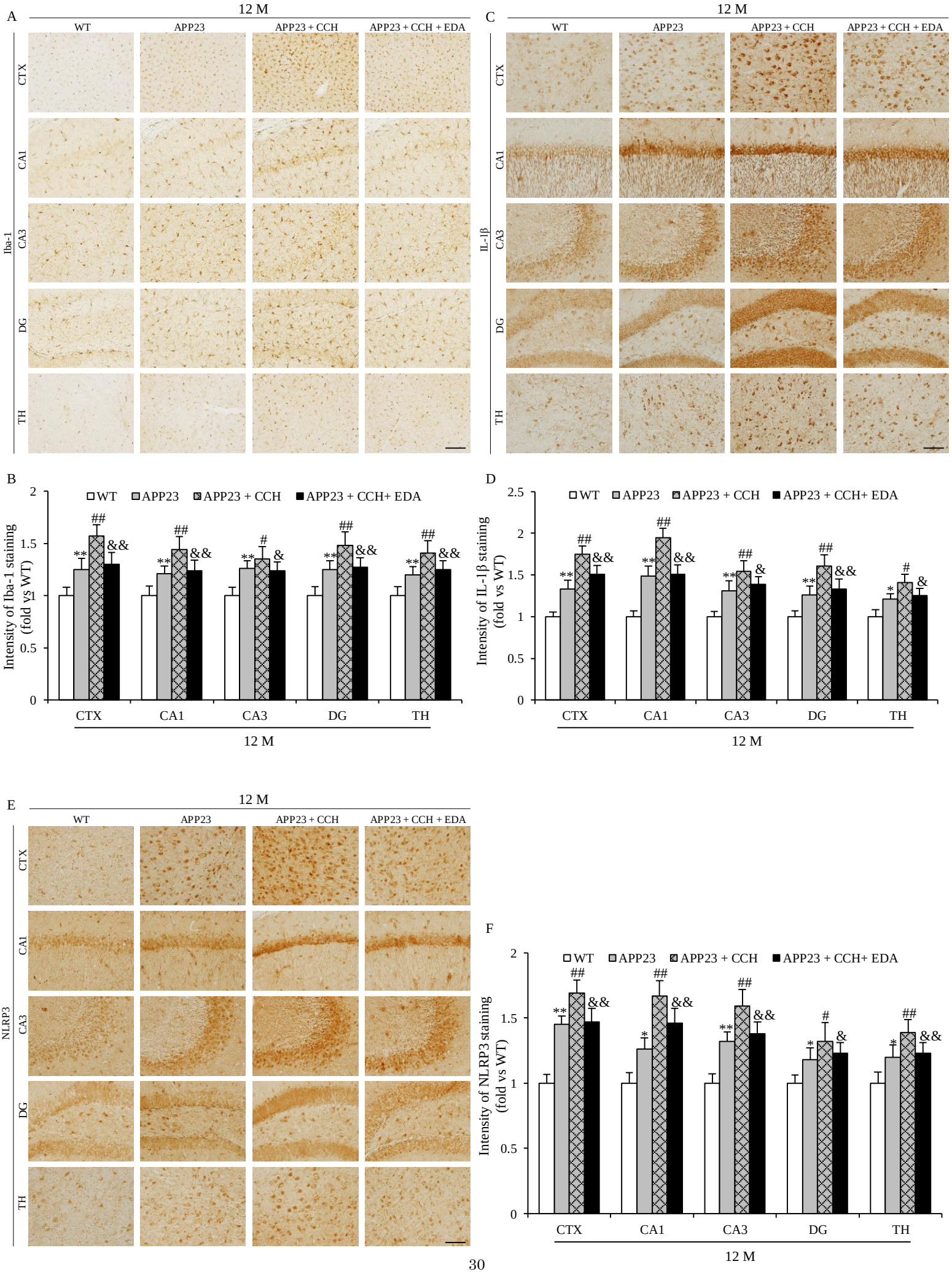
A
12 M
WT
APP23
APP23 + CCH
APP23 + CCH + EDA
Iba-1
CTX
CA1
CA3
DG
TH
C
12 M
WT
APP23
APP23 + CCH
APP23 + CCH + EDA
IL-1β
CTX
CA1
CA3
DG
TH
B
WT
APP23
APP23 + CCH
APP23 + CCH+ EDA
Intensity of Iba-1 staining (fold vs WT)
CTX
CA1
CA3
DG
TH
12 M
D
WT
APP23
APP23 + CCH
APP23 + CCH+ EDA
Intensity of IL-1β staining (fold vs WT)
CTX
CA1
CA3
DG
TH
12 M
E
12 M
WT
APP23
APP23 + CCH
APP23 + CCH + EDA
NLRP3
CTX
CA1
CA3
DG
TH
F
WT
APP23
APP23 + CCH
APP23 + CCH+ EDA
Intensity of NLRP3 staining (fold vs WT)
CTX
CA1
CA3
DG
TH
12 M